Increasing Photostability of Inverted Nonfullerene Organic Solar Cells by using Fullerene Derivative Additives

Increasing Photostability of Inverted Nonfullerene Organic Solar Cells by using Fullerene Derivative Additives

Marcella Günther, Dominic Blätte, Anna Lena Oechsle[‡], Sergio Sánchez Rivas, Amir Abbas Yousefi Amin, Peter Müller-Buschbaum[‡,†], Thomas Bein, Tayebeh Ameri[#]**

Department of Chemistry and Center for NanoScience (CeNS), Ludwig-Maximilians-Universität (LMU), Butenandtstr. 5-13, 81377 Munich, Germany

Keywords: ternary organic solar cells, photostability, zinc oxide, nonfullerene acceptors, fullerenes, photocatalytic activity

ABSTRACT

Organic solar cells recently achieved efficiencies of over 18% and are well on their way to practical applications, but still considerable stability issues need to be overcome. One major problem emerges from the electron transport material zinc oxide (ZnO), which is mainly used in the inverted device architecture and decomposes many high performance nonfullerene acceptors due to its photocatalytic activity. In this work we add three different fullerene derivatives – $PC_{71}BM$, ICMA and BisPCBM – to an inverted binary PBDB-TF:IT-4F system in order to suppress the photocatalytic degradation of IT-4F on ZnO via the radical scavenging abilities of the fullerenes. We demonstrate that the addition of 5% fullerene not only increases the performance of the binary PBDB-TF:IT-4F system, but also significantly improves the device lifetime under UV illumination in inert atmosphere. While the binary devices lose 20% of their initial efficiency after only 3 hours, this time is increased fivefold for the most promising ternary devices with ICMA. We attribute this improvement to a reduced photocatalytic decomposition of IT-4F in the ternary system, which results in a decreased recombination. We propose that the added fullerenes protect the IT-4F by acting as a sacrificial reagent, and thereby suppress the trap state formation. Furthermore, we show that the protective effect of the most promising fullerene ICMA is transferable to two other binary systems PBDB-TF:BTP-4F and PTB7-Th:IT-4F. Importantly, this effect can also increase the air stability of PBDB-TF:IT-4F. This work demonstrates that the addition of fullerene derivatives is a transferable and straightforward strategy to improve the stability of organic solar cells.

1. INTRODUCTION

With efficiencies reaching over 18%,[1–3] organic solar cells (OSCs) have become serious competitors for state-of-the art inorganic solar cells. This is especially true because their properties such as lightweight, low cost, sustainable materials and flexibility allow them to open entirely new markets. For commercial applications, however, not only the efficiency has to be convincing, but also the stability must be sufficiently high, which is not yet the case for many high-performance OSC systems. A major degradation influence, which of course cannot be avoided, is light. Nearly all organic solar cells show an initial fast degradation when being exposed to light the first time, which is referred to as a burn-in.[4,5]

This initial light-induced degradation can have two fundamentally different causes of either morphological or molecular nature. Morphological changes occur when the energy introduced into the OSC by light causes diffusion[6] or recrystallization of components, thus resulting in a loss of the optimal interpenetrating network of the bulk heterojunction (BHJ).[7–9] Molecular changes occur when the incident light breaks chemical bonds directly[10] or activates reactions of the components with each other,[11,12] with impurities,[13] or with interlayers.[14]

An inverted architecture is normally considered being more stable for devices containing fullerene acceptors.[15,16] However, for nonfullerene acceptors the inverted geometry brings up new stability issues. Especially, the electron transport layer (ETL) ZnO, which is commonly used in inverted devices, can cause stability problems.[17] ZnO is known as photocatalyst for the degradation of organic compounds and, for example, is used for water purification.[18–20] Upon irradiation with UV light, electron-hole pairs are created in the ZnO, which then can either react directly with adsorbed pollutants or form reactive oxygen species (e.g. $^{\bullet}OH$, $^{\bullet}O_2^-$) with the surrounding water, which act as mobile, potent oxidizing agents and decompose dissolved pollutants.[20]

This photocatalytic reactivity of ZnO, which is very desirable for water purification, can have a detrimental effect in organic solar cells.[14,21,22] The organic molecules, which are located adjacent to the ZnO layer, can be reduced or oxidized directly due to the photoinduced charge carriers in ZnO.[20] Furthermore, as a result of the manufacturing process, water and oxygen are adsorbed on the ZnO surface,[23,24] which again can form mobile, reactive oxygen species that attack the active materials.[25]

Nonfullerene acceptors have been shown to be particularly susceptible to the destructive influence of ZnO,[14,21] since they usually contain end groups like indandione (e.g. ITIC, IT-4F, IEICO-4F) or rhodanine (e.g. IDFBR) that are connected to the core by a non-aromatic double bond, which is vulnerable to addition reactions. It has been demonstrated that IT-4F, ITIC and IEICO-4F films coated on a ZnO substrate undergo complete photobleaching in less than 100 hours when exposed to UV illumination.[14] A more detailed investigation with ITIC revealed that the excitation of ZnO causes an addition reaction of radical oxygen species to the vinyl bond in ITIC and dimerization of ITIC was also detected.[21] In a solar cell, this process causes a loss of absorption and more importantly, the degraded molecules can act as charge traps and thus as recombination centers.

The use of UV filters in front of the solar cells could solve the degradation problem by suppressing the photocatalytic activity of ZnO, however, this is not a reasonable option due to ZnO suffering from the so-called light-soaking issue.[26] Photovoltaics containing ZnO as ETL need UV illumination to passivate defect states on the surface of the ZnO and to reach their optimum performance. It is assumed that those defect states originate from the chemisorption of oxygen on the ZnO surface, which traps electrons from the ZnO conduction band by forming O_2^- species and thus creates a depletion layer and band bending next to the interface.[27] This results in a barrier for

electron injection or extraction and consequently in an s-shaped current density-voltage curve (*JV*-curve), which causes a reduced fill factor. UV illumination generates electron-hole pairs in the ZnO which help desorbing the oxygen due to the holes recombining with O_2^- and forming O_2 again.[27] This results in a decrease of the injection/extraction barrier and the recovery of the performance of the solar cell.

A more promising way to suppress the detrimental influence of ZnO on the absorbing materials is to introduce a protective interlayer between ETL and absorbing layer.[22,28,29] For example, a thin pyrene-bodipy based layer on top of ZnO was shown to significantly increase the device lifetime under illumination for both PBDB-TF:IT-4F and PTB7-Th:$PC_{71}BM$ systems, respectively.[22]

However, this method of using a protective layer increases the complexity in manufacturing the solar cells due to the additional layer and thereby would also increase the potential cost of the OSC manufacturing. A much simpler approach would be to suppress the UV aging due to ZnO by directly adding a protective third compound to the binary absorber mixture of the active layer. Promising candidates for this approach are fullerenes, since they are well known radical scavengers[30,31] and already established materials for OSCs.

In this work, we use a ternary approach to investigate the influence of three different fullerene derivatives, namely $PC_{71}BM$, ICMA and BisPCBM, on the UV stability of inverted binary solar cells consisting of the donor PBDB-TF and the acceptor IT-4F (all systematic names can be found in the experimental part). The fullerene derivatives are found to significantly slow down the UV-induced aging of the binary system, mainly due to decreased losses of the fill factor. It is shown that the addition of fullerenes reduces the formation of defect states, which emerge due to the photocatalytic degradation of IT-4F on the electron transport layer ZnO. In the present work, a

mechanism is proposed that explains the protective effect of the fullerenes with their radical scavenging abilities, suppressing the detrimental influence of ZnO.

2. RESULTS AND DISCUSSION

2.1 Performance of ternary OSCs

In Figure 1a the molecular structures of the used materials are illustrated. The corresponding energy levels are provided in Figure S1. Binary and ternary organic solar cells were built in an inverted architecture with ZnO as the ETL and MoO_x as the hole transport layer (HTL), as illustrated in Figure 1b. For the binary blend, the polymeric donor PBDB-TF and the small molecule acceptor IT-4F were used in a 1:1 weight ratio. For the ternary blends 5 wt% of $PC_{71}BM$, ICMA or BisPCBM were added, respectively. A weight ratio of 5% was found to achieve the highest power conversion efficiency (*PCE*) values for all three ternary blends, as illustrated in Figure S2.

Inverted binary OSCs with PBDB-TF:IT-4F have been reported to yield champion efficiencies between 12% to 13% ,[14,32] however, since the aim of this study was to compare the device stability of binary and ternary solar cells, the *PCE* was not extensively optimized, but all cells were built following a standardized procedure.

The *PCE* distribution of the binary and the three different ternary systems is shown in Figure 1c, the corresponding distributions of the open-circuit voltage (V_{OC}), short-circuit current density (J_{SC}) and fill factor (*FF*) can be found in Figure S3. For each system, 30 individual cells fabricated in three different experimental batches are presented. The associated average and record photovoltaic performance parameters are summarized in Table 1. The binary reference system on average achieved an efficiency of 8.8%, with a V_{OC} of 0.83 V, a J_{SC} of 16.9 $mAcm^{-2}$ and a *FF* of 64%. The addition of 5% fullerene derivative had a positive effect for all three studied fullerenes and resulted in an average *PCE* improvement of 6%, 10%, and 7% for $PC_{71}BM$, ICMA and BisPCBM, respectively, compared to the binary system. This improvement originates mainly from an

increased J_{SC} and *FF*, whereas the V_{OC} remains nearly unchanged with the addition of the third component. As can be seen from the absorption coefficients of the binary and ternary blends in Figure S4, the fullerenes do not significantly improve the absorption of the different solar cells. However, in the external quantum efficiency (EQE) spectra, shown in Figure 1d, a difference becomes visible. In the wavelength region from 500 to 800nm, the EQE of all ternary cells is higher than that of the binary cell, with the ternary ICMA showing the strongest increase. This region corresponds to the absorption range of IT-4F (Figure S4), and thus suggests that the fullerenes improve charge transport from the acceptor. This effect probably also accounts for the enhanced *FF*, since the addition of fullerenes is known to result in an increased and more balanced charge carrier mobility.[33,34]

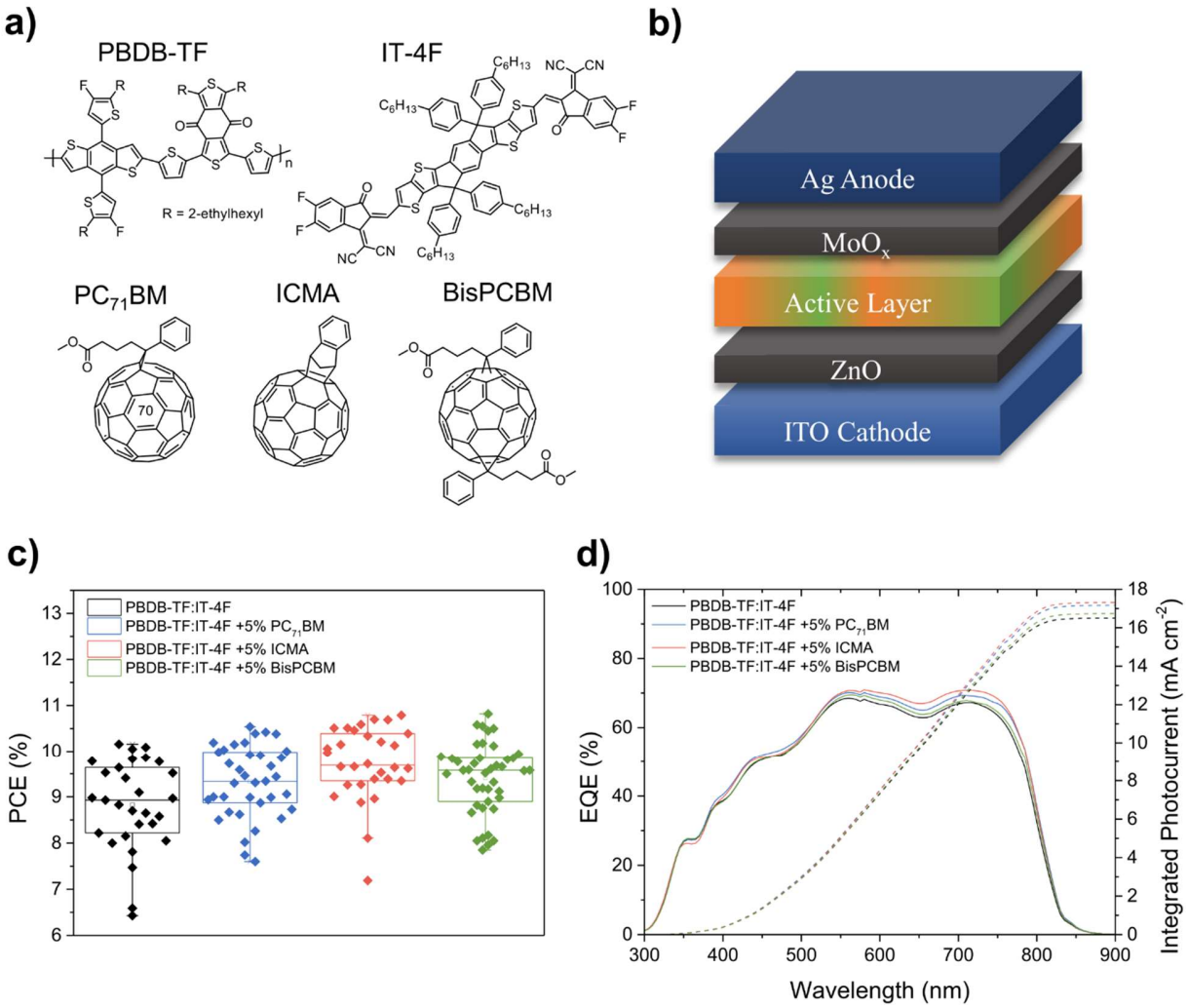

Figure 1. a) Chemical structures of all used active layer materials, b) inverted device architecture of all built OSCs, c) *PCE* distribution (from 30 individual solar cells each) of the binary and the three ternary systems with added fullerenes as indicated, and d) the respective external quantum efficiency spectra (EQE) of the best cells with corresponding integrated photocurrents.

Table 1. Maximum and average values (in brackets) of performance parameters for binary and ternary devices from 30 cells conducted in three different experimental rounds.

	PCE (%)	V_{OC} (V)	J_{SC} (mA cm^{-2})	*FF* (%)
PBDB-TF:IT-4F	10.2 (8.8 ± 1.0)	0.85 (0.83 ± 0.02)	17.3 (16.9 ± 1.3)	69 (64 ± 4)
PBDB-TF:IT-4F + 5% $PC_{71}BM$	10.5 (9.3 ± 0.8)	0.83 (0.82 ± 0.01)	17.7 (17.4 ± 0.5)	71 (66 ± 4)
PBDB-TF:IT-4F + 5% ICMA	10.8 (9.7 ± 0.8)	0.83 (0.83 ± 0.01)	17.7 (17.4 ± 0.5)	73 (69 ± 4)
PBDB-TF:IT-4F + 5% BisPCBM	10.8 (9.4 ± 0.8)	0.84 (0.83 ± 0.01)	17.8 (17.0 ± 1.0)	72 (67 ± 4)

2.2 UV stability of binary and ternary cells

The UV stability of binary and ternary cells was examined by exposing them to a continuous UV illumination in a nitrogen atmosphere. A UV LED emitting at 365nm was used as the light source and its intensity was calibrated to match the intensity of the UV part (300-400nm) of one sun radiation. At regular time intervals, a *JV*-curve was measured under a white light LED to determine the change in the performance of the solar cells. The spectra of all used light sources can be found in Figure S5.

In Figure 2a the aging of the four different systems during 30 hours of continuous UV illumination is presented. For every system three individual cells were averaged, and all data points were normalized to the performance of the respective fresh devices. The *PCE* curves for all devices show a typical burn-in behavior[4] with an exponential decay of the efficiency in the first few hours. However, it is evident that the addition of the fullerenes significantly reduces the burn-in, and thus increases the device lifetime in all cases. The lifetime is usually defined as the time after which the device has lost 20% of its initial efficiency (so called T_{80} lifetime).[15] For the binary cells this time is only three hours, while it is more than doubled by the addition of $PC_{71}BM$ (7h) and BisPCBM (6h). For the cells with ICMA even a fivefold T_{80} lifetime (16h) is achieved.

The degradation of the *PCE* for all four systems is mainly from *FF* losses, with rather small losses in V_{OC} and J_{SC}. The fill factor is also the parameter that experiences the strongest stability improvement through the addition of the fullerenes, with ICMA showing the most pronounced effect and $PC_{71}BM$ and BisPCBM behaving very similar. Interestingly, the stability of the V_{OC} and J_{SC} values is also improved to the greatest extent by the addition of ICMA, followed by $PC_{71}BM$ and BisPCBM with a similar effect.

To examine if the observed stabilization effect scales with the amount of added fullerene, ternary devices with different ratios of the most promising candidate ICMA were built and aged under the same conditions for 120 hours. The degradation over time for V_{OC} and *FF*, which are the two performance parameters with the most distinct aging effect, is shown in Figure 2b. The corresponding *PCE* and J_{SC} curves can be found in Figure S6. It is obvious that the stabilizing effect of ICMA depends on the fullerene content, but already amounts as small as 1.25wt% result in a significantly improved stability. Furthermore, the stabilizing effect seems to saturate with an increasing ratio of ICMA. Since the performance of fresh devices decreases when 10% or more ICMA is added, 5% ICMA was chosen as the best trade-off between reaching a high device efficiency and a long device stability.

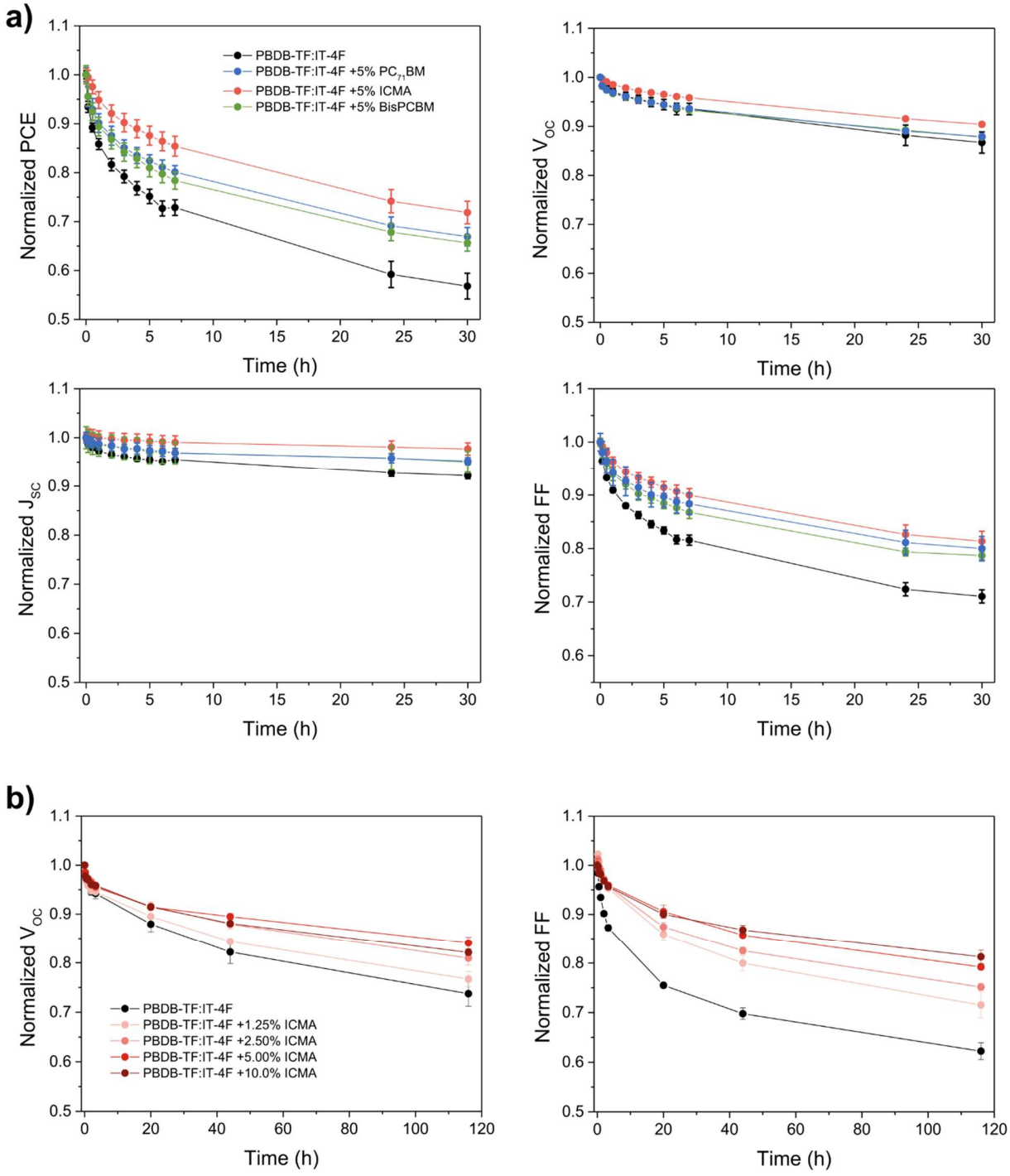

Figure 2. a) UV stability of the photovoltaic parameters of binary and ternary devices (averaged over 3 devices each) as a function of time. b) UV stability of V_{OC} and *FF* as a function of time for binary PBDB-TF:IT-4F cells and ternary cells with different ratios of ICMA.

2.3 Characterization of fresh and aged devices

To investigate the origin of the UV instability of the binary system and to understand the stabilizing effect of the three added fullerenes, various characterization methods were performed to compare the fresh devices with the corresponding devices aged for 24 hours under UV illumination.

Already a first look at the *JV*-curves of fresh and aged devices shows a striking difference. As depicted in Figure 3a, the *JV*-curves of the three fresh ternary devices are very similar to the one of the fresh binary devices. However, the aged binary devices not only show a much higher fill factor loss (Figure 2a), but above all a strongly increased series resistance. On average, the fresh binary devices have a series resistance (R_S) of 6.7 Ω cm^2, whereas aged devices show a series resistance of 19.6 Ω cm^2, which corresponds to an increase of almost 200%. Meanwhile, R_S only increased by about 60% for the aged ternary devices compared to the fresh ones. The strong increase of R_S in binary devices indicates that the aging might be interface-related and that the fullerenes have a protective function in the ternary devices.

To learn more about the observed losses in J_{SC}, UV-vis spectroscopy and EQE measurements were performed for fresh and aged devices. As shown in Figure S7a, all systems experience a small loss in absorption, which is most pronounced for the binary system, and which mainly seems to come from the absorption region of IT-4F (550-800nm). Remarkably, the EQEs of the binary fresh and aged devices (Figure S7b) do not reflect this loss. While the EQEs of the ternary systems remain nearly unchanged after the UV exposure, the aged binary system shows a small loss over the entire wavelength range, what is more clearly visible when the EQE difference is plotted, as in Figure S7c. Since the main aging induced current losses in all systems occur at around maximum power point (see Figure 3a) and not for the J_{SC}, voltage-dependent EQE was performed

additionally. By measuring the cells biased with 0.6V, the changes in current density for fresh and aged cells become more obvious, as depicted in Figure 3b (see Figure S7d for EQE differences). The EQEs of all fresh devices biased with 0.6V are very similar, however, after 24h of UV illumination the binary and ternary EQEs differ greatly from each other. They all show a loss over the whole wavelength region, but this loss is much larger for the binary system. This finding suggests that although during the aging the IT-4F is partly attacked, it is not the absorption loss but another dominant process that reduces the exciton harvesting all over the spectrum. This process apparently is slowed down by the addition of the fullerene derivatives.

Furthermore, since the main *PCE* losses for all systems originate from the fill factor, light intensity dependent *JV*-measurements and Fourier-transform photocurrent spectroscopy (FTPS) were carried out in order to study the recombination behavior of fresh and aged devices.[35]

In Figure 3c the light intensity dependence of the V_{OC} is depicted for all four systems, fresh and after 24 hours of UV aging. According to $V_{OC} \sim nkT / e \cdot \ln(I)$ the V_{OC} is linearly dependent on the natural logarithm of the light intensity I and the slope corresponds to the product of the ideality factor n, the Boltzmann constant k and the temperature T.[36] An ideality factor of one hereby signifies a recombination mechanism that is exclusively bimolecular, while for only monomolecular recombination the ideality factor is two.[37] The fresh devices all have a rather similar ideality factor between 1.24 and 1.27, and all devices show an increased ideality factor after exposure to UV illumination. However, the extent of this increase is quite different. While the ideality factor of the binary system increases from 1.26 to 1.43, the ternary systems with ICMA and BisPCBM exhibit 40% less increase of n compared to the binary one. The ideality factor of the ternary system with $PC_{71}BM$ increases in a similar way as the binary one.

The FTPS results of the fresh and aged devices are depicted in Figure 3d. The spectral region from 900 to 1450nm (sub-band gap) can be divided into two parts.[38,39] The part between 900-1000nm is attributed to the absorption of band tail states and is mainly related to the energetic disorder of the bulk. The part from 1000nm upwards, which has a much lower slope, can be assigned to the absorption of defect states. The FTPS results of all fresh devices are quite similar, but for the aged devices differences emerge in both regions. In the absorption region of the band tail states, all aged systems show a small shift to lower energies, suggesting an increased energetic disorder. The more remarkable feature, however, is the change in the defect state region. Here, the aged binary system shows a strongly increased current from defect state absorption, while the aged ternary devices feature a substantially smaller increase. We note that the extent of this increase corresponds to the observed ranking in the stability of the systems with the ICMA device being the most stable device and showing the least increase.

These findings suggest that a large share of the binary system aging is caused by increased trap-assisted recombination and that the addition of the fullerenes, especially ICMA, partly suppresses this effect.

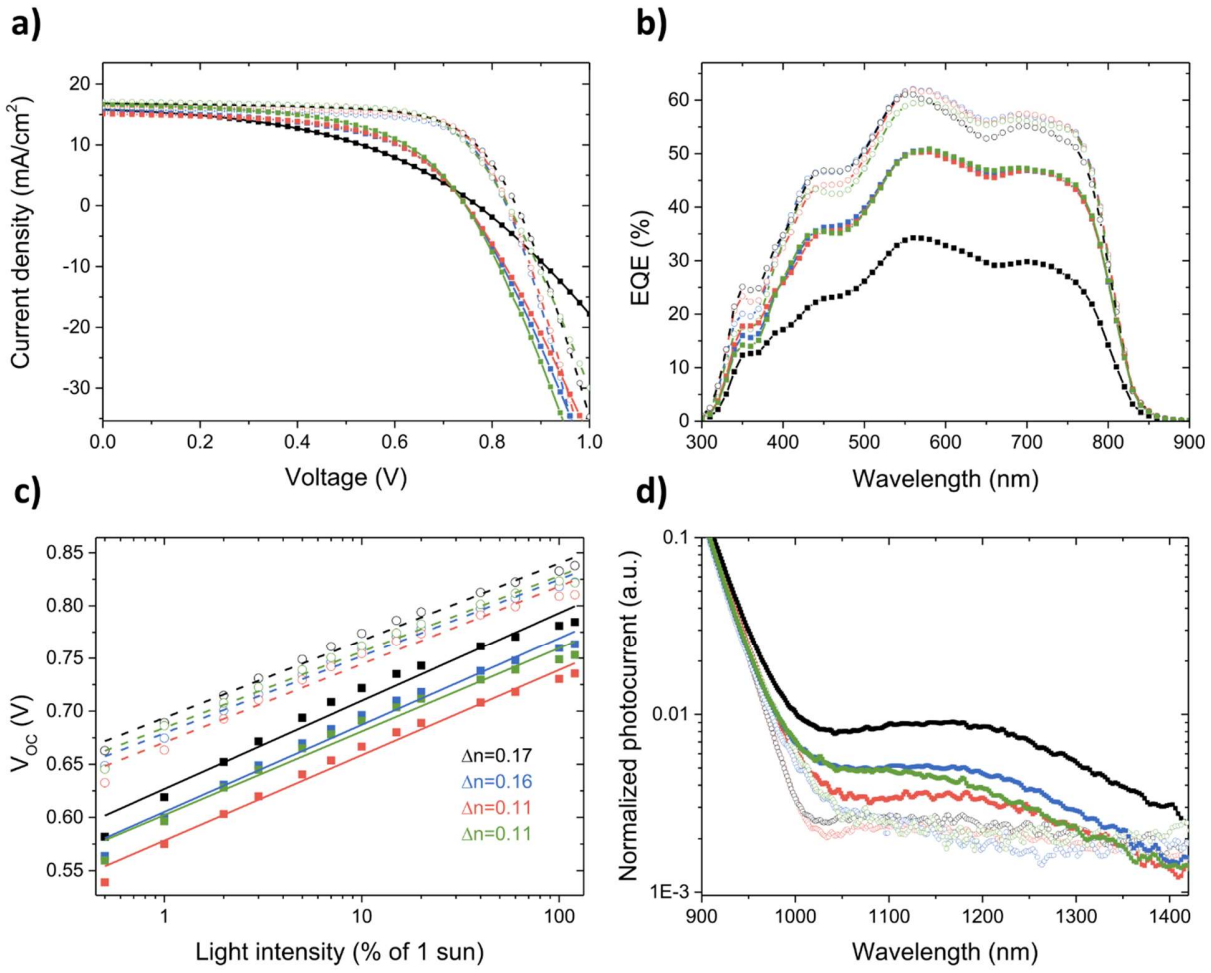

Figure 3. Characterization of the fresh binary/ternary devices and of the same devices aged for 24 hours under UV light. a) *JV* characteristics under illumination, b) voltage-dependent EQE-spectra at a bias of 0.6V, c) light intensity dependence of V_{OC}, and d) FTPS measurements of binary PBDB-TF:IT-4F (black) and ternary devices with added $PC_{71}BM$ (blue), ICMA (red), and BisPCBM (green). Fresh devices are shown with dashed lines/empty symbols and 24h UV aged ones with solid lines/filled symbols.

To examine whether morphological changes are the reason for the emergence of traps, grazing-incidence wide-angle and small-angle X-ray scattering (GIWAXS and GISAXS) measurements were performed for the binary and ternary blends. The 2D GIWAXS data of the fresh and aged

blends are shown in Figure S8, the corresponding out-of-plane and in-plane cake cuts are presented in Figure 4a and Figure 4b. In all GIWAXS patterns, the (100) diffraction peak at $q \approx 3.2\text{nm}^{-1}$ is visible, indicating a high crystallinity of the polymer PBDB-TF.[40] Additionally, the in-plane cuts show a broad diffraction peak between $q \approx 12\text{nm}^{-1}$ and 18nm^{-1}, which is attributed to the (010) Bragg peak of crystalline PBDB-TF.[40] No significant differences are visible in the line cuts, neither between the binary and ternary devices nor between the fresh and aged ones. To additionally investigate possible changes on larger length scales addressing domain sizes and distributions, an in-depth analysis of the 2D GISAXS data was performed by modeling the intensity curves resulting from horizontal line cuts in the Yoneda region. To account for the different length-scales of the domains, the data is modeled with three cylindrically-shaped substructures, according to the local monodisperse approximation (LMA) in the framework of the distorted wave Born approximation (DWBA).[41–43] The 2D GISAXS data and all LMA-DWBA fit parameters can be found in Figure S9 and Table S1. The intensity cuts and their modeled fits, as shown in Figure 4c, are very similar for fresh and aged films of the binary and ternary blends. A closer look at the fit parameters (Table S1) confirms that indeed radius and center-to-center domain distances for the three different length-scales are the same within the error bars. For the medium sized substructures, it is noticeable that the intensity-weighted proportion in the fit increases somewhat after the aging. However, since this is the case for all four systems, this increase cannot be the reason for the different aging behavior. Therefore, both GIWAXS and GISAXS measurements indicate that no morphological changes are responsible for the improved aging behavior of the fullerene containing devices. Interestingly, such stability of the PBDB-TF:IT-4F film morphology is in contrast to similar systems studied in operando experiments. For example, Wienhold et al. observed in PBDB-

T-SF:IT-4F OSCs a J_{SC} driven aging, which was caused by a reduction of interfaces per cross section area.[44]

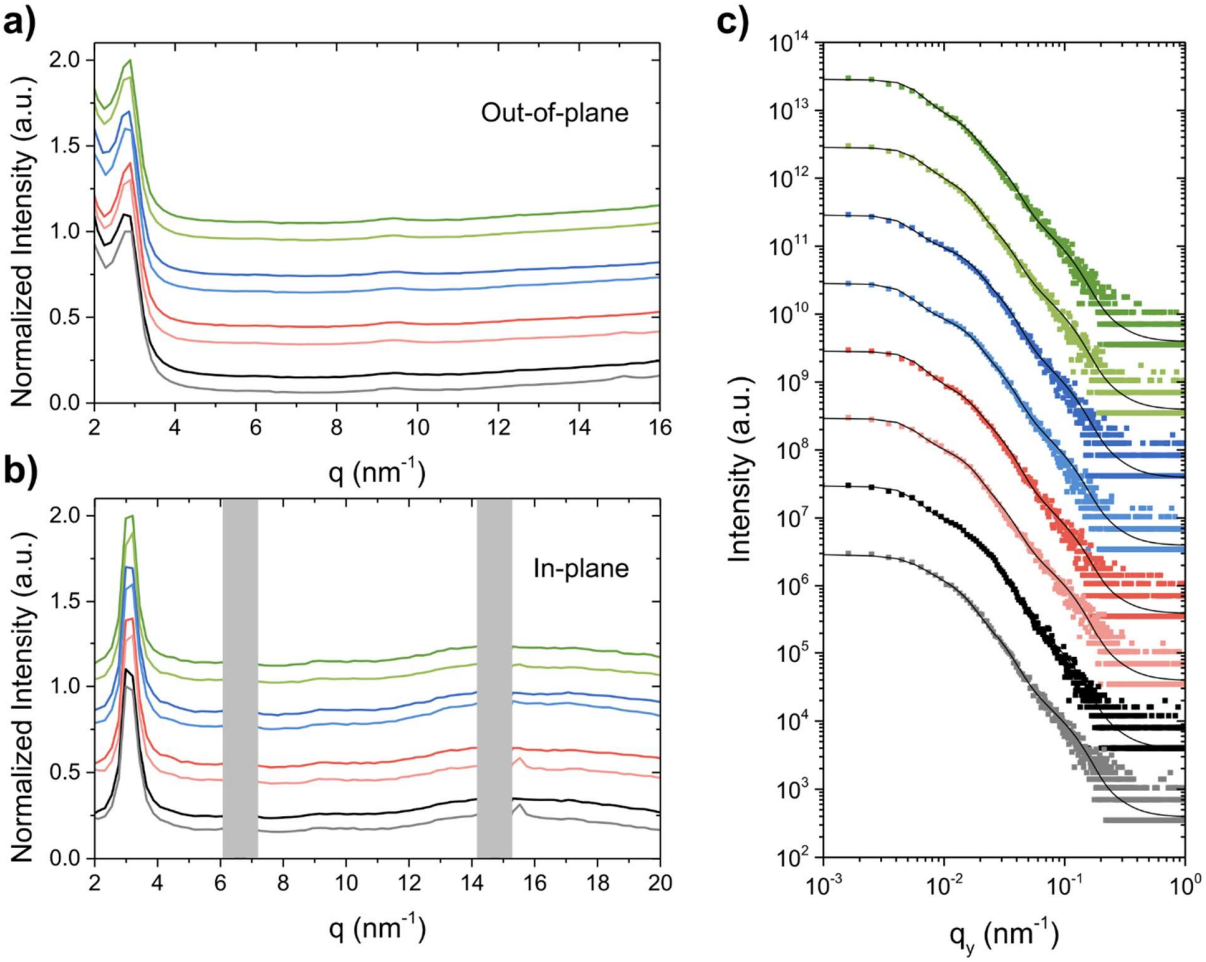

Figure 4. Normalized a) out-of-plane and b) in-plane cake cuts of the 2D GIWAXS data and c) horizontal line cuts of 2D GISAXS data at the critical angle of 0.1° (symbols) and the corresponding fits of binary PBDB-TF:IT-4F (black lines) and ternary devices with added $PC_{71}BM$ (blue), ICMA (red), and BisPCBM (green). Fresh devices are shown with light colors and 24h UV aged ones with darker colors. The curves are shifted along the *y*-axis for clarity of the presentation.

2.4 Origin of UV aging and explanation for the protective effect of the fullerenes

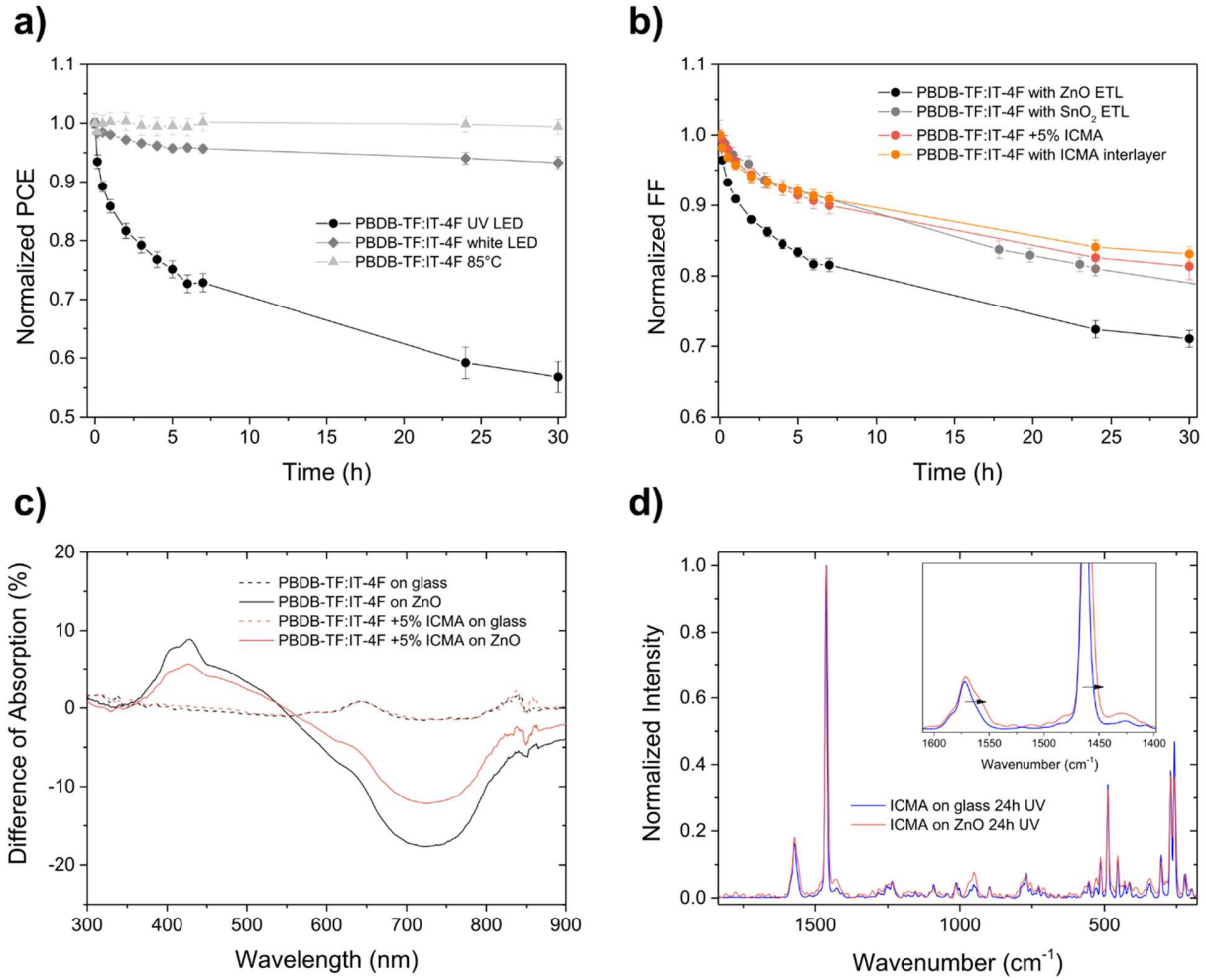

Figure 5. a) *PCE* as a function of time for binary PBDB-TF:IT-4F devices aged for 30 hours under different conditions. Devices were aged in nitrogen atmosphere either under a UV LED calibrated to the UV part of one sun radiation (black), under a white light LED calibrated to one sun radiation (grey) or in the dark on a hotplate at 85°C (light grey). For each condition the average of three individual devices is shown. b*) FF* as a function of time during continuous UV illumination for binary devices with a ZnO ETL (black), binary devices with a SnO_2 ETL (grey), ternary ICMA devices (red), and binary devices with an ICMA interlayer between ZnO and BHJ (orange). c) Difference of UV-vis spectra of fresh blends and blends aged for 24 hours under UV

illumination for a binary blend on glass (dotted black) and on ZnO (solid black) and for a ternary ICMA blend on glass (dotted red) and on ZnO (solid red). d) Raman spectra of ICMA that was aged on glass (blue) and on ZnO (red) as a film, scraped off and measured as powder.

In this work, the GIWAXS and GISAXS results indicate that the different aging behavior of binary and ternary systems is not morphology related. However, there might be morphological changes that are not clearly visible in GIWAXS and GISAXS, for example on very small scales or in amorphous regions. Moreover, adding fullerenes as the third compound has been shown to stabilize the microstructure of binary blends against recrystallization and phase separation and thus increasing the stability.[45,46]

Therefore, in order to further ensure that the origin of the aging process of the binary PBDB-TF:IT-4F system is not morphological, the UV aging was compared to two other aging conditions. On the one hand, the binary system under nitrogen was exposed to a white light LED, which has been calibrated to one sun (≈100 mW cm^{-2}) and therefore emits a much higher overall intensity than the used UV LED (≈4.6 mW cm^{-2}). The spectra of the used LEDs can be found in Figure S5. On the other hand, the binary device was thermally aged at 85°C under nitrogen atmosphere. In contrast to chemical aging, degradation of the binary blend that is caused by morphological changes, such as recrystallization or diffusion, should mainly depend on the amount of energy absorbed. Consequently, if the aging resulted from morphological modifications, the aging due to the white LED or the elevated temperature would show a similar or worse behavior as the UV LED aging, since the overall absorbed energy is higher (see absorption spectra in Figure S4).

However, such a similar behavior cannot be observed in the obtained time-dependent *PCE* curves, as shown in Figure 5a. The corresponding V_{OC}, J_{SC} and *FF* curves can be found in Figure S10. The binary cells exposed to the white light LED and to the increased temperature both show

a considerably slower loss of efficiency than the one exposed to the UV LED. This clearly demonstrates that the mechanism of the observed aging under UV illumination is dependent on the wavelength of the LED. In addition to the GIWAXS and GISAXS findings, it is taken as a strong indication for the UV aging being a molecular rather than a morphological degradation process, in contrast to other findings about white light aging of PBDB-TF:IT-4F devices.[8]

One possible molecular degradation pathway of active layer materials, already shown by several groups,[47–49] arises from the presence of the additive DIO, which was also used for the manufacturing of the cells in this work. In particular, it was demonstrated that residual DIO under the influence of UV illumination can form radicals, that attack and decompose the acceptor material ITIC.[49] This mechanism could also be transferable to the ITIC derivative IT-4F used here. To investigate whether the observed aging trends of binary and ternary cells are related to the additive used, binary PBDB-TF:IT-4F cells and ternary PBDB-TF:IT-4F:ICMA cells were prepared without DIO (see Table S2 for performance parameters) and aged under the same conditions. As visible in Figure S11, the aging trends for binary and ternary cells with and without DIO are quite comparable. The binary cells without DIO age slightly slower than with DIO and this difference could well be due to a detrimental influence of the additive. However, more importantly, the fullerene ICMA has the same stabilizing effect with and without DIO, which proves that ICMA slows down an aging process that is clearly not related to the additive DIO.

Other possible causes of chemical and non-morphological aging processes are linked to the interfaces with the transport layers. To investigate this, binary devices were built with SnO_2 instead of ZnO as an ETL. SnO_2 has a larger band gap than ZnO and does not absorb at the wavelength used for the UV aging, as shown in the UV-vis spectra in Figure S12. Therefore, UV-induced aging processes, which originate from the ETL, can be excluded when using SnO_2. The

performance parameters of these cells can be found in Table S3. The SnO_2-based cells were built using the same recipe as for the ZnO-based cells, although the efficiency is worse, mainly due to a smaller J_{SC} and *FF*. Afterward, they were aged under the same conditions as those used for the ZnO-based cells. Remarkably, their aging behavior is different from that of the ZnO-based binary cells, as shown in Figure 5b and Figure S13. Especially, the aging of the *FF* is significantly slowed down and resembles more the curve of the ternary cell with ICMA. However, there seems to be another process, that causes the V_{OC} to age faster and therefore decrease the stability of the system. Nevertheless, this slower aging of the binary system on SnO_2 is a strong indication that the ZnO interlayer is the reason for a photocatalytic degradation process in the binary devices.

To prove that the fullerene implemented in the bulk photoactive layer really suppresses this proposed degradation at the interface, binary cells were built with a thin interlayer of ICMA in between ZnO and photoactive layer (for details see experimental section). The device performance after UV aging is also shown in Figure 5b and Figure S13. It is evident that the aging behavior of the ternary ICMA devices and the devices with ICMA interlayer is very similar and that in both cases the stability compared to the binary devices is improved in the same way. This finding proves that ICMA suppresses an interface related degradation process, which even works when ICMA is mixed into the active layer.

In order to understand what this UV-induced molecular degradation process at the interface looks like and what causes it, the UV-vis spectra of the fresh and aged thin films of the binary and ternary ICMA blend were more closely examined. In Figure 5c we present the difference in absorption of the fresh and aged films, normalized to the intensities of the fresh films. Interestingly, the respective films on glass (dotted lines) show no change in absorption after aging, indicating a good UV stability of the pristine molecules. However, if a ZnO layer is present underneath the

films, the absorption is changed after UV illumination. Both the binary and the ternary blend show an absorption loss between 550-850nm (the absorption range of IT-4F), that is more pronounced for the binary blend, and an absorption increase between 350-550nm. Such an absorption loss of IT-4F or ITIC containing blends on top of ZnO has also been observed by other groups and has been attributed to photocatalytic degradation of the nonfullerene acceptor on the ZnO.[14,50] The absorption increase between 350nm and 550nm is assumed to be caused by the degradation products.[14] Obviously, the addition of ICMA, respectively the other fullerenes, suppresses the ZnO-induced photocatalytic degradation of IT-4F.

To get an indication of how the fullerenes protect the other active layer materials and whether they themselves are altered in the process, thin layers of ICMA on glass and on ZnO were aged under UV, scraped off and the obtained powder was analyzed with Raman spectroscopy. The two spectra, shown in Figure 5d, are very similar and show the same peaks as pristine ICMA, namely several small peaks between 700cm^{-1} and 1480cm^{-1}, which can be attributed to various vibrations of C-H groups and two larger features from vibrations of C_{60} at 1462cm^{-1} and 1572cm^{-1}, where the former comes from the symmetric C=C stretching.[51] A closer look at this region reveals that for the ICMA aged on ZnO those two peaks experience a broadening towards smaller wave numbers, indicating the slight expansion of some bonds in the C_{60}, which could for example happen due to an addition reaction of an electronegative functional group to a C=C bond. Thus, these results are a clear evidence that ZnO can cause UV-induced molecular changes to a fullerene.

Combining these observations with the finding that the main difference in UV stability of binary and ternary cells comes from a different trap density, the following explanation for the stabilizing effect of the fullerenes is proposed and schematically depicted in Figure 6: Upon UV illumination, an electron-hole pair is excited in the ZnO, which can interact with species that are adsorbed on

the surface of ZnO.[23] This results in the generation of reactive oxygen species,[20] symbolized here as an OH-radical, which can then attack the vulnerable vinyl bonds of the IT-4F (Figure 6a), and thus destroy the conjugation in the small molecule acceptor.[14] The degraded IT-4F firstly absorbs less, which leads to a small decrease in J_{SC} of the binary cell. Secondly, and more importantly, the degraded IT-4F acts as a recombination center and therefore strongly reduces the fill factor of the binary devices. The added fullerene, depicted here as ICMA, acts as a radical scavenger and can catch several of those reactive oxygen species,[30,31] and thus, protects the IT-4F molecule from chemical degradation (Figure 6b). The fullerenes with their large delocalized systems and good electron accepting properties can stabilize radicals and, therefore, do not act as recombination center.

To understand the different effects of the three used fullerenes on the UV stability of the binary blend (ICMA>$PC_{71}BM$>BisPCBM), the location of the fullerenes in the ternary blend must be considered. For this reason, contact angle measurements of all pristine components were performed with water and glycerol and the surface energy was calculated according to the Wu model.[52] The results are summarized in Table S4. The surface energy of ICMA (40.3 mN m^{-1}) is much higher than the values of PBDB-TF (18.0 mN m^{-1}) and IT-4F (24.5 mN m^{-1}), and therefore it is expected to demix from the host system during film preparation and accumulate at the ZnO interface, while the lower surface energy components accumulate at the air surface to reduce the total energy.[53] Consequently, ICMA can trap the reactive oxygen species on the ZnO surface more efficiently and the protective effect is high. On the other hand, the surface energies of BisPCBM (27.8 mN m^{-1}) and $PC_{71}BM$ (30.6 mN m^{-1}) are only somewhat higher than those of the binary host, which means that they do not demix to the same extent and thus show a smaller protective effect than ICMA.

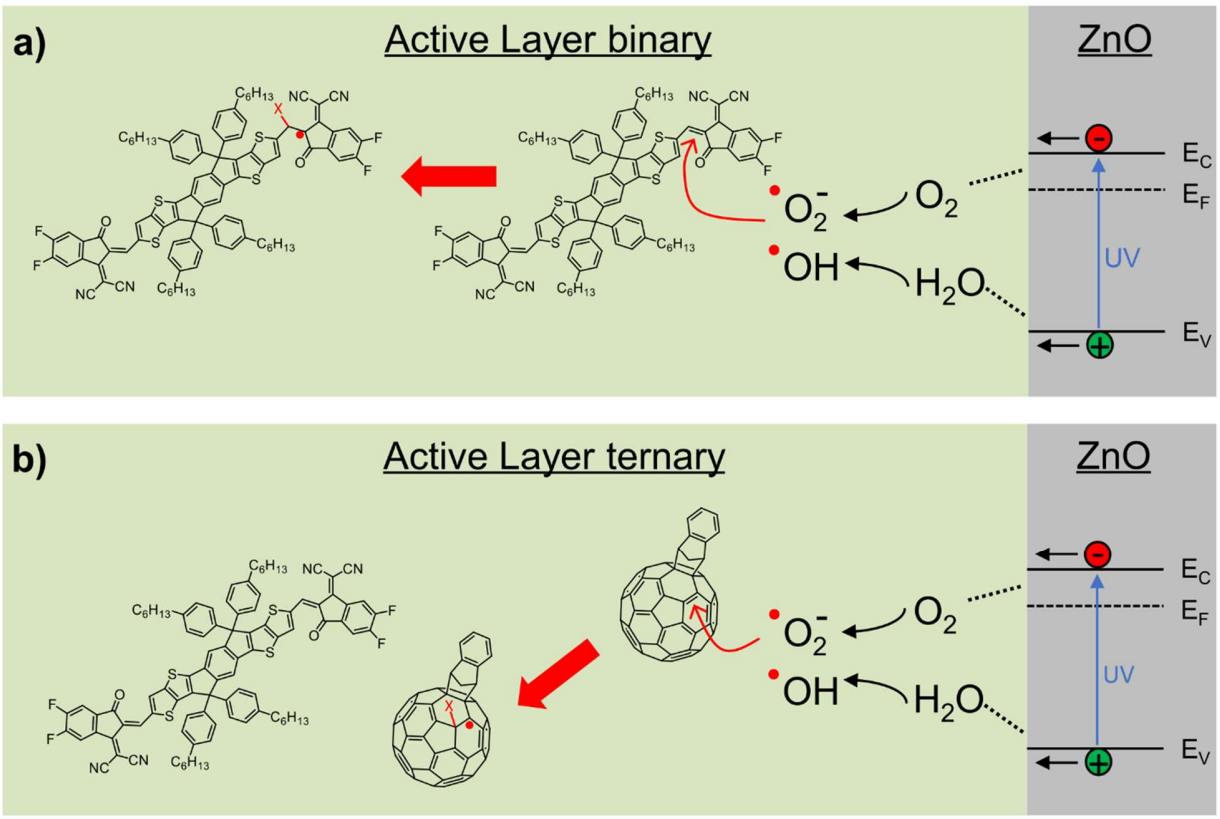

Figure 6. Scheme of the proposed mechanism for the ZnO-induced aging process in binary and ternary devices. UV light generates an electron-hole-pair in the ZnO, which reacts with species adsorbed on the ZnO surface. Reactive oxygen species, as for example OH-radicals, are created, which then can attack the vulnerable vinyl bonds of IT-4F (a). The deteriorated IT-4F acts as recombination center. ICMA protects IT-4F as sacrificial reagent and radical scavenger (b). Due to the large delocalized system, it can stabilize radicals, thus not acting as recombination center.

2.5 Transferability of the protective effect

In order to examine whether the protective effect of the fullerenes is transferable, two other binary systems were chosen. On the one hand, PBDB-TF was combined with another nonfullerene acceptor BTP-4F and on the other hand IT-4F was combined with another polymer PTB7-Th. In

both cases, corresponding ternary devices containing additionally 5% ICMA were also built. The average performance parameters of all devices can be found in Table S5. Next, binary and ternary devices then were exposed to the same UV aging conditions as described above for the PBDB-TF:IT-4F system.

As visible from Figure 7a, the PBDB-TF:BTP-4F binary cells show the exact same aging behavior as the PBDB-TF:IT-4F system and, most importantly, the addition of ICMA has the same stabilizing effect, which mainly comes from reduced losses in *FF* and V_{OC} (Figure S14). The UV stability of the PTB7-Th:IT-4F binary devices, shown in Figure 7b, demonstrate also a burn-in behavior which is comparable to the PBDB-TF:IT-4F system and furthermore, the added ICMA in the ternary cells slows down the aging. However, in this system the protective effect of the fullerene is not as strong as for PBDB-TF:IT-4F and PBDB-TF:BTP-4F, which could be related to a different miscibility of the PTB7-Th polymer with the acceptors IT-4F and ICMA.

Remarkably, this protective effect can not only be transferred to other materials systems, but even to other aging conditions. Binary devices based on PBDB-TF:IT-4F and the corresponding ternary devices with additional 5% ICMA were exposed to air for 24 hours in the dark. The *PCE* as a function of time, presented in Figure 7c, clearly reveals that the addition of ICMA significantly slows down the *PCE* loss, which likewise mainly originates from smaller losses in *FF* and V_{OC}, while the J_{SC} remains nearly unchanged in both devices (Figure S14). In agreement with our photostability results, the better air-stability of the ternary device also suggest that ICMA acts as a radical scavenger for oxygen radicals diffusing into the active layer and consequently suppresses the oxidation of the ZnO surface.[54] However, further investigations, which are beyond the scope of this work, will be necessary to elucidate the detailed mechanism of this effect.

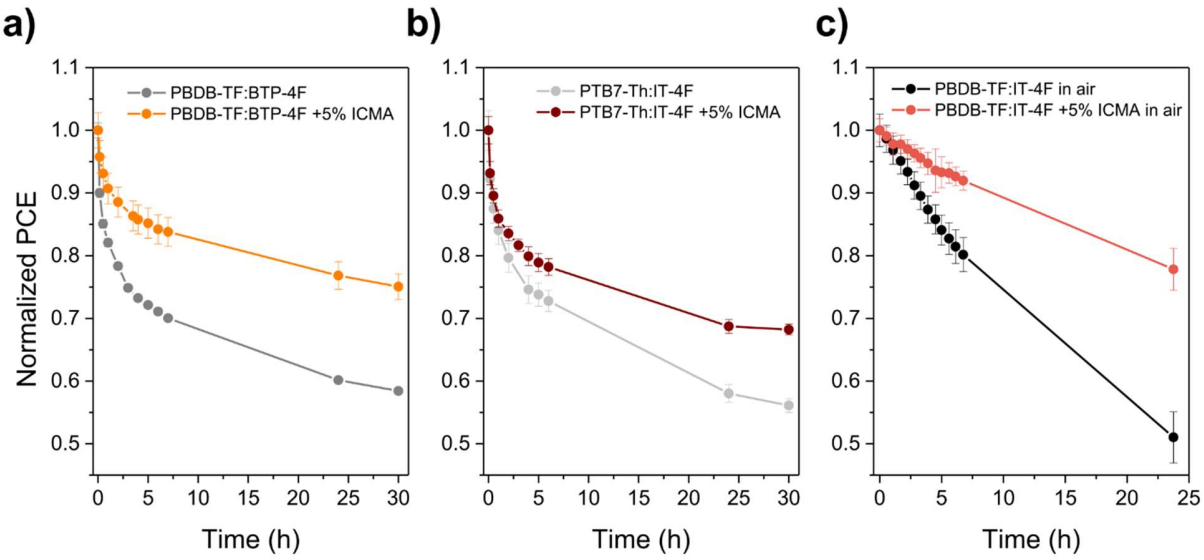

Figure 7. a,b) UV stability of the *PCE* as a function of time for binary PBDB-TF:BTP-4F devices and PTB7-Th:IT-4F devices and the corresponding ternary devices containing additionally 5% ICMA. c) Air stability of the *PCE* as a function of time for binary PBDB-TF:IT-4F devices and the corresponding ternary device with 5% ICMA. For all systems four individual devices were averaged and normalized to the respective fresh device.

3. CONCLUSIONS

In conclusion, we successfully demonstrated that the efficiency and UV photostability of a PBDB-TF:IT-4F based OSC can be improved by simply incorporating different fullerene derivatives into the bulk heterojunction, resulting in an up to fivefold increased lifetime without affecting the active layer morphology or negatively impacting on the *PCE*. Upon UV illumination, devices without fullerenes showed a rapidly decreasing fill factor due to increasing monomolecular recombination, which is attributed to the photocatalytic degradation of IT-4F at the ZnO interface. Based on the light intensity-dependent V_{OC} and FTPS results, the fullerenes protect IT-4F from the detrimental influence of ZnO by acting as radical scavengers and, thus, suppressing the emergence

of trap states. Furthermore, we showed that the protective effect of fullerenes is transferable to OSCs based on different polymers and nonfullerene acceptors and even significantly increases the air stability. This work illustrates that a ternary approach – compared to additional protective interlayers – provides a simple and versatile method to protect nonfullerene acceptors from the photocatalytic activity of ZnO and increase the photostability of inverted organic solar cells.

4. EXPERIMENTAL SECTION

Materials. ITO substrates with 15 Ωcm^2 were purchased from Kintec. The ZnO nanoparticle dispersion (Avantama-N10) was purchased from Avantama AG. Poly[(2,6-(4,8-bis(5-(2-ethylhexyl)thiophen-2-yl)-benzo[1,2-b:4,5-b′]dithiophene))-alt-(5,5-(1′,3′-di-2-thienyl-5′,7′-bis(2-ethylhexyl)benzo[1′,2′-c:4′,5′-c′]dithiophene-4,8-dione))] (denoted PBDB-TF, sometimes called PBDB-T-2FF or PM6), 3,9-bis(2-methylene-((3-(1,1-dicyanomethylene)-6,7-difluoro)-indanone))-5,5,11,11-tetrakis(4-hexylphenyl)-dithieno[2,3-d:2′,3′-d′]-s-indaceno[1,2-b:5,6-b′]dithiophene (IT-4F) and 2,2'-((2Z,2'Z)-((12,13-bis(2-ethylhexyl)-3,9-diundecyl-12,13-dihydro-[1,2,5]thiadiazolo[3,4-e]thieno[2",3'':4',5']thieno[2',3':4,5]pyrrolo[3,2-g]thieno[2',3':4,5]thieno [3,2-b]indole-2,10-diyl)bis(methanylylidene))bis(5,6-difluoro-3-oxo-2,3-dihydro-1H-indene-2,1-diylidene))dimalononitrile (denoted BTP-4F, sometimes called Y6) were provided by Solarmer. Poly[4,8-bis(5-(2-ethylhexyl)thiophen-2-yl)benzo[1,2-b;4,5-b']dithiophene-2,6-diyl-alt-(4-(2-ethylhexyl)-3-fluorothieno[3,4-b]thiophene-)-2-carboxylate-2-6-diyl)] (denoted PTB7-Th, sometimes called PCE10) was purchased from 1-Material. [6,6]-Phenyl-C71-butyric acid methyl ester ($PC_{71}BM$), indene-C_{60} monoadduct (ICMA) and bis(1-[3-(methoxycarbonyl)propyl]-1-phenyl)-[6,6]C62 (BisPCBM) with a purity of >99% were obtained from Solenne BV. Chlorobenzene, 1,8-diiodooctane (DIO), and 1-chloronaphthalene were purchased from Sigma Aldrich.

Device Fabrication. ITO substrates were cleaned with detergent and ultrasonicated in water, acetone and isopropanol for 10 min. The substrates were then dried under a nitrogen flow and plasma cleaned for 20 min. A 40nm ZnO layer was spin coated (1400rpm for 60s) and annealed for 10min at 120°C in air. Subsequently, the substrates were moved to a nitrogen glovebox. For the active layer solutions, all compounds were dissolved separately, then mixed and stirred

overnight. For the PBDB-TF:IT-4F binary active layer a 1:1 weight ratio with a total concentration of 20 mg ml^{-1} in chlorobenzene was prepared. For the corresponding ternary active layers, 5wt% of $PC_{71}BM$, ICMA or BisPCBM was added (dissolved in chlorobenzene with 20 mg mL^{-1} concentration), resulting in a ratio of approximately 1:1:0.05. The ICMA solution was heated to 70°C to completely dissolve prior to mixing. At a time 30min before spin coating, v/v 0.5% DIO was added and then all active layers were dynamically spin coated with a two-step program, first 900 rpm for 5s followed by 4000rpm for 60s. For the binary devices with an ICMA interlayer a 20 mg mL^{-1} ICMA solution at 70°C was dynamically spin coated (1000rpm for 60s) on top of ZnO, followed by an annealing at 120°C for 15min. Subsequently, the PBDB-TF:IT-4F layer was spin coated as explained before. For the PTB7-Th:IT-4F binary active layer a 1:1.5 weight ratio with a total concentration of 20 mg ml^{-1} in chlorobenzene was prepared, and for the corresponding ternary active layer 5wt% of ICMA was added (20 mg mL^{-1} in chlorobenzene). Also, v/v 0.5% DIO was added 30min before spin coating the active layer (1500rpm for 60s). For the PBDB-TF:BTP-4F binary active layer a 1:1.2 weight ratio with a total concentration of 16 mg mL^{-1} in chloroform was prepared, and for the corresponding ternary active layer 5wt% of ICMA was added (16mg mL^{-1} in chloroform). 30min before spin coating v/v 0.5% 1-chloronaphthalene was added and the mixture was spin coated with 3000rpm for 30s. Finally, on top of all devices 10nm of MoO_x and 100nm of Ag were evaporated through a mask.

Characterization Techniques. *JV*-measurements were performed using a Keithley 2401 source-measure unit and a Newport ABA solar simulator, which was calibrated to AM1.5G using a Fraunhofer silicon diode. UV-vis spectra of the thin films on glass substrates were recorded with a Perkin Elmer Lambda 1050 instrument, using an integrating sphere and an InGaAs detector. EQE measurements were performed with a home-built setup using a 150 W Xe short arc lamp

(LOT Oriel) combined with a monochromator (Horiba microHR) and two Si-diodes (Hamamatsu) to calibrate the photon flux and compensate for light intensity fluctuations. For voltage-dependent EQE measurements a potentiostat (Metrohm Autolab) was used to apply voltage and simultaneously measure current. Light intensity dependent *JV*-curves were measured using a Keithley 2401 source-measure unit and a white light LED as light source. A Si-photodiode was used to control the light intensity. FTPS measurements were done with a modified Bruker Vertex 70 FTIR instrument by focusing light from a tungsten halogen lamp through a CaF_2 beam splitter with integrated gold mirrors to illuminate the devices under short-circuit conditions. The current from the devices was amplified with a FEMTO DHPCA-100 current amplifier, passed through an analog-to-digital converter, and fed back to the FTIR instrument for Fourier transformation. Every measurement was averaged over 10000 scans for noise reduction and then scaled to the respective EQE signals, which were obtained separately. FT-Raman powder measurements were done with a RAM II extension of the Bruker Vertex 70 with a germanium detector at an excitation wavelength of 1064 nm and a laser power of 50mW. GIWAXS and GISAXS measurements were performed at the P03 beamline at DESY[55] (Hamburg, Germany) at an energy of 12.85 keV. For GIWAXS a Pilatus 300k detector (Dectris) was used and the data were obtained at an incident angle of 0.32° and a sample detector distance (SDD) of 287mm. 2D-GIWAXS data were corrected and evaluated with the software GIXSGUI.[56] For GISAXS a Lambda pixel detector (DESY) was used and the data were obtained at an incident angle of 0.32° and an SDD of 3554mm. Data evaluation was performed with the open source Python program DPDAK. Horizontal line cuts were made at the critical angle of PBDB-TF (0.1° for 12.85 keV).

Stability Testing. All device photostability tests were performed in a nitrogen filled glovebox with water and oxygen levels <1ppm. The illumination with UV light or white light LED was

performed through the glass substrate and a shadow mask with 6.25 mm^2. The devices were aged under a 365nm UV LED (Thorlabs), which was calibrated with a Si-diode (Hamamatsu) to match the UV part of AM1.5G (300-400nm, corresponds to 4.6 mW cm^{-2}). For the *JV*-measurements a Keithley 2401 was used and the devices were illuminated with a white light LED, which was also calibrated to 1 sun with a Si-diode. For the air stability tests, devices were aged under dark condition in air at a constant temperature of 20°C.

ASSOCIATED CONTENT

The following file is available free of charge.

Figure S1-S14 and Table S1-S5 regarding details about device performance, absorption measurements, GIWAXS and GISAXS studies, spectra of light sources, contact angle measurements, and additional stability studies (PDF)

AUTHOR INFORMATION

Corresponding Author

*Email: tayebeh.ameri@ed.ac.uk

*Email: marcella.guenther@lmu.de

Present Addresses

ǂ Physik-Department, Lehrstuhl für Funktionelle Materialien, Technische Universität München, James-Franck-Str. 1, 85748 Garching, Germany

† Heinz Maier-Leibnitz-Zentrum (MLZ), Technische Universität München, Lichtenbergstr. 1, 85748 Garching, Germany

Institute for Materials and Processes, Chemical Engineering, University of Edinburgh, Sanderson Building, Robert Stevenson Road, EH9 3FB, UK

Author Contributions

M.G. built devices, performed the opto-electronic characterization and wrote the manuscript. T.A. supervised the device preparation and characterization and discussed the results. D.B. performed and evaluated FTPS and Raman measurements. A.L.O. performed and evaluated the GISAXS and GIWAXS measurements. P.M.B. supervised the evaluation of GISAXS and GIWAXS measurements. S.S.R. built devices and did air stability measurements. A.A.Y.A and T.B. discussed the results and contributed to the manuscript. The manuscript was corrected and commented on by all authors. All authors have given approval to the final version of the manuscript.

ACKNOWLEDGMENT

The authors gratefully acknowledge funding by the Deutsche Forschungsgemeinschaft (DFG, German Research Foundation) under Germany´s Excellence Strategy – EXC 2089/1 – 390776260 (e-conversion) and funding by the Bavarian Ministry of Science (Solar Technologies go Hybrid – SolTech). T. A. acknowledges the financial support of the German Research Foundation (DFG project with grant number of AM 519/1-1). We thank Dr. Matthias Schwartzkopf for help with setting up the DESY beamline.

REFERENCES

(1) Lin, Y.; Firdaus, Y.; Isikgor, F. H.; Nugraha, M. I.; Yengel, E.; Harrison, G. T.; Hallani, R.; El-Labban, A.; Faber, H.; Ma, C.; Zheng, X.; Subbiah, A.; Howells, C. T.; Bakr, O. M.; McCulloch, I.; Wolf, S. D.; Tsetseris, L.; Anthopoulos, T. D. Self-Assembled Monolayer Enables Hole Transport Layer-Free Organic Solar Cells with 18% Efficiency and Improved Operational Stability. *ACS Energy Lett.* **2020**, *5* (9), 2935–2944. DOI: 10.1021/acsenergylett.0c01421.

(2) Liu, Q.; Jiang, Y.; Jin, K.; Qin, J.; Xu, J.; Li, W.; Xiong, J.; Liu, J.; Xiao, Z.; Sun, K.; Yang, S.; Zhang, X.; Ding, L. 18% Efficiency Organic Solar Cells. *Science Bulletin* **2020**, *65* (4), 272–275. DOI: 10.1016/j.scib.2020.01.001.

(3) Lin, Y.; Nugraha, M. I.; Firdaus, Y.; Scaccabarozzi, A. D.; Aniés, F.; Emwas, A.-H.; Yengel, E.; Zheng, X.; Liu, J.; Wahyudi, W.; Yarali, E.; Faber, H.; Bakr, O. M.; Tsetseris, L.; Heeney, M.; Anthopoulos, T. D. A Simple n-Dopant Derived from Diquat Boosts the Efficiency of Organic Solar Cells to 18.3%. *ACS Energy Lett.* **2020**, *5* (12), 3663–3671. DOI: 10.1021/acsenergylett.0c01949.

(4) Mateker, W. R.; McGehee, M. D. Progress in Understanding Degradation Mechanisms and Improving Stability in Organic Photovoltaics. *Adv. Mater.* **2017**, *29* (10). DOI: 10.1002/adma.201603940.

(5) Chochos, C. L.; Leclerc, N.; Gasparini, N.; Zimmerman, N.; Tatsi, E.; Katsouras, A.; Moschovas, D.; Serpetzoglou, E.; Konidakis, I.; Fall, S.; Lévêque, P.; Heiser, T.; Spanos, M.; Gregoriou, V. G.; Stratakis, E.; Ameri, T.; Brabec, C. J.; Avgeropoulos, A. The Role of Chemical Structure in Indacenodithienothiophene-alt -benzothiadiazole Copolymers for High Performance Organic Solar Cells with Improved Photo-stability through Minimization of Burn-in Loss. *J. Mater. Chem. A* **2017**, *5* (47), 25064–25076. DOI: 10.1039/C7TA09224E.

(6) Zhang, C.; Mumyatov, A.; Langner, S.; Perea, J. D.; Kassar, T.; Min, J.; Ke, L.; Chen, H.; Gerasimov, K. L.; Anokhin, D. V.; Ivanov, D. A.; Ameri, T.; Osvet, A.; Susarova, D. K.; Unruh, T.; Li, N.; Troshin, P.; Brabec, C. J. Overcoming the Thermal Instability of Efficient Polymer Solar Cells by Employing Novel Fullerene-Based Acceptors. *Adv. Energy Mater.* **2017**, *7* (3), 1601204. DOI: 10.1002/aenm.201601204.

(7) Li, N.; Perea, J. D.; Kassar, T.; Richter, M.; Heumueller, T.; Matt, G. J.; Hou, Y.; Güldal, N. S.; Chen, H.; Chen, S.; Langner, S.; Berlinghof, M.; Unruh, T.; Brabec, C. J. Abnormal Strong Burn-in Degradation of Highly Efficient Polymer Solar Cells Caused by Spinodal Donor-Acceptor Demixing. *Nat Commun* **2017**, *8.* DOI: 10.1038/ncomms14541.

(8) Du, X.; Heumueller, T.; Gruber, W.; Almora, O.; Classen, A.; Qu, J.; He, F.; Unruh, T.; Li, N.; Brabec, C. J. Unraveling the Microstructure-Related Device Stability for Polymer Solar Cells Based on Nonfullerene Small-Molecular Acceptors. *Adv. Mater.* **2020**, *32* (16). DOI: 10.1002/adma.201908305.

(9) Schaffer, C. J.; Palumbiny, C. M.; Niedermeier, M. A.; Jendrzejewski, C.; Santoro, G.; Roth, S. V.; Müller-Buschbaum, P. A Direct Evidence of Morphological Degradation on a Nanometer Scale in Polymer Solar Cells. *Adv. Mater.* **2013**, *25* (46), 6760–6764. DOI: 10.1002/adma.201302854.

(10) Street, R. A.; Northrup, J. E.; Krusor, B. S. Radiation Induced Recombination Centers in Organic Solar Cells. *Phys. Rev. B* **2012**, *85* (20). DOI: 10.1103/PhysRevB.85.205211.

(11) Distler, A.; Sauermann, T.; Egelhaaf, H.-J.; Rodman, S.; Waller, D.; Cheon, K.-S.; Lee, M.; Guldi, D. M. The Effect of PCBM Dimerization on the Performance of Bulk Heterojunction Solar Cells. *Adv. Energy Mater.* **2014**, *4* (1), 1300693. DOI: 10.1002/aenm.201300693.

(12) Heumueller, T.; Mateker, W. R.; Distler, A.; Fritze, U. F.; Cheacharoen, R.; Nguyen, W. H.; Biele, M.; Salvador, M.; Delius, M. von; Egelhaaf, H.-J.; McGehee, M. D.; Brabec, C. J. Morphological and Electrical

Control of Fullerene Dimerization Determines Organic Photovoltaic Stability. *Energy Environ. Sci.* **2016**, *9* (1), 247–256. DOI: 10.1039/C5EE02912K.
(13) Jacobs, I. E.; Wang, F.; Bedolla Valdez, Z. I.; Ayala Oviedo, A. N.; Bilsky, D. J.; Moulé, A. J. Photoinduced Degradation from Trace 1,8-Diiodooctane in Organic Photovoltaics. *J. Mater. Chem. C* **2018**, *6* (2), 219–225. DOI: 10.1039/C7TC04358A.
(14) Jiang, Y.; Sun, L.; Jiang, F.; Xie, C.; Hu, L.; Dong, X.; Qin, F.; Liu, T.; Hu, L.; Jiang, X.; Zhou, Y. Photocatalytic Effect of ZnO on the Stability of Nonfullerene Acceptors and its Mitigation by SnO_2 for Nonfullerene Organic Solar Cells. *Mater. Horiz.* **2019**, *6* (7), 1438–1443. DOI: 10.1039/C9MH00379G.
(15) Gevorgyan, S. A.; Madsen, M. V.; Roth, B.; Corazza, M.; Hösel, M.; Søndergaard, R. R.; Jørgensen, M.; Krebs, F. C. Lifetime of Organic Photovoltaics: Status and Predictions. *Adv. Energy Mater.* **2016**, *6* (2). DOI: 10.1002/aenm.201501208.
(16) Wang, W.; Schaffer, C. J.; Song, L.; Körstgens, V.; Pröller, S.; Indari, E. D.; Wang, T.; Abdelsamie, A.; Bernstorff, S.; Müller-Buschbaum, P. In Operando Morphology Investigation of Inverted Bulk Heterojunction Organic Solar Cells by GISAXS. *J. Mater. Chem. A* **2015**, *3* (16), 8324–8331. DOI: 10.1039/C5TA01109D.
(17) Sorrentino, R.; Kozma, E.; Luzzati, S.; Po, R. Interlayers for Non-Fullerene Based Polymer Solar Cells: Distinctive Features and Challenges. *Energy Environ. Sci.* **2021**, *375* (11). DOI: 10.1039/D0EE02503H.
(18) Youssef, Z.; Colombeau, L.; Yesmurzayeva, N.; Baros, F.; Vanderesse, R.; Hamieh, T.; Toufaily, J.; Frochot, C.; Roques-Carmes, T.; Acherar, S. Dye-Sensitized Nanoparticles for Heterogeneous Photocatalysis: Cases Studies with TiO_2, ZnO, Fullerene and Graphene for Water Purification. *Dyes and Pigments* **2018**, *159*, 49–71. DOI: 10.1016/j.dyepig.2018.06.002.
(19) Baruah, S.; K. Pal, S.; Dutta, J. Nanostructured Zinc Oxide for Water Treatment. *Nanosci Nanotechnol.--Asia* **2012**, *2* (2), 90–102. DOI: 10.2174/2210681211202020090.
(20) Lam, S.-M.; Sin, J.-C.; Abdullah, A. Z.; Mohamed, A. R. Degradation of Wastewaters Containing Organic Dyes Photocatalysed by Zinc Oxide: a Review. *Desalin. Water Treat.* **2012**, *41* (1-3), 131–169. DOI: 10.1080/19443994.2012.664698.
(21) Park, S.; Son, H. J. Intrinsic Photo-Degradation and Mechanism of Polymer Solar Cells: the Crucial Role of Non-Fullerene Acceptors. *J. Mater. Chem. A* **2019**, *7* (45), 25830–25837. DOI: 10.1039/C9TA07417A.
(22) Soultati, A.; Verykios, A.; Panagiotakis, S.; Armadorou, K.-K.; Haider, M. I.; Kaltzoglou, A.; Drivas, C.; Fakharuddin, A.; Bao, X.; Yang, C.; Yusoff, A. R. B. M.; Evangelou, E. K.; Petsalakis, I.; Kennou, S.; Falaras, P.; Yannakopoulou, K.; Pistolis, G.; Argitis, P.; Vasilopoulou, M. Suppressing the Photocatalytic Activity of Zinc Oxide Electron-Transport Layer in Nonfullerene Organic Solar Cells with a Pyrene-Bodipy Interlayer. *ACS Appl. Mater. Interfaces* **2020**, *12* (19), 21961–21973. DOI: 10.1021/acsami.0c03147.
(23) Wöll, C. The Chemistry and Physics of Zinc Oxide Surfaces. *Progress in Surface Science* **2007** (82), 55–120. DOI: 10.1016/J.PROGSURF.2006.12.002.
(24) Noei, H.; Qiu, H.; Wang, Y.; Löffler, E.; Wöll, C.; Muhler, M. The Identification of Hydroxyl Groups on ZnO Nanoparticles by Infrared Spectroscopy. *Phys. Chem. Chem. Phys.* **2008**, *10* (47), 7092–7097. DOI: 10.1039/b811029h.
(25) Liu, B.; Han, Y.; Li, Z.; Gu, H.; Yan, L.; Lin, Y.; Luo, Q.; Yang, S.; Ma, C.-Q. Visible Light–Induced Degradation of Inverted Polymer:Nonfullerene Acceptor Solar Cells: Initiated by the Light Absorption of ZnO Layer. *Sol. RRL* **2020**, *35.* DOI: 10.1002/solr.202000638.
(26) Liang, Z.; Zhang, Q.; Jiang, L.; Cao, G. ZnO Cathode Buffer Layers for Inverted Polymer Solar Cells. *Energy Environ. Sci.* **2015**, *8* (12), 3442–3476. DOI: 10.1039/C5EE02510A.

(27) Wilken, S.; Parisi, J.; Borchert, H. Role of Oxygen Adsorption in Nanocrystalline ZnO Interfacial Layers for Polymer–Fullerene Bulk Heterojunction Solar Cells. *J. Phys. Chem. C* **2014**, *118* (34), 19672–19682. DOI: 10.1021/jp506641m.
(28) Polydorou, E.; Botzakaki, M.; Drivas, C.; Seintis, K.; Sakellis, I.; Soultati, A.; Kaltzoglou, A.; Speliotis, T.; Fakis, M.; Palilis, L. C.; Kennou, S.; Fakharuddin, A.; Schmidt-Mende, L.; Davazoglou, D.; Falaras, P.; Argitis, P.; Krontiras, C. A.; Georga, S. N.; Vasilopoulou, M. Insights into the Passivation Effect of Atomic Layer Deposited Hafnium Oxide for Efficiency and Stability Enhancement in Organic Solar Cells. *J. Mater. Chem. C* **2018**, *6* (30), 8051–8059. DOI: 10.1039/C8TC02243G.
(29) Sadeghianlemraski, M.; Harding, C. R.; Welch, G. C.; Aziz, H. Significant Photostability Enhancement of Inverted Organic Solar Cells by Inserting an N-Annulated Perylene Diimide (PDIN-H) between the ZnO Electron Extraction Layer and the Organic Active Layer. *ACS Appl. Energy Mater.* **2020**, *3* (12). DOI: 10.1021/acsaem.0c01587.
(30) Bosi, S.; Da Ros, T.; Spalluto, G.; Prato, M. Fullerene Derivatives: an Attractive Tool for Biological Applications. *Eur. J. Med. Chem.* **2003**, *38* (11-12), 913–923. DOI: 10.1016/j.ejmech.2003.09.005.
(31) Zeynalov, E. B.; Allen, N. S.; Salmanova, N. I. Radical Scavenging Efficiency of Different Fullerenes C_{60}–C_{70} and Fullerene Soot. *Polym. Degrad. Stab.* **2009**, *94* (8), 1183–1189. DOI: 10.1016/j.polymdegradstab.2009.04.027.
(32) Ji, G.; Zhao, W.; Wei, J.; Yan, L.; Han, Y.; Luo, Q.; Yang, S.; Hou, J.; Ma, C.-Q. 12.88% Efficiency in Doctor-Blade Coated Organic Solar Cells through Optimizing the Surface Morphology of a ZnO Cathode Buffer Layer. *J. Mater. Chem. A* **2019**, *7* (1), 212–220. DOI: 10.1039/C8TA08873J.
(33) Yu, R.; Yao, H.; Cui, Y.; Hong, L.; He, C.; Hou, J. Improved Charge Transport and Reduced Nonradiative Energy Loss Enable Over 16% Efficiency in Ternary Polymer Solar Cells. *Adv. Mater.* **2019**, *31* (36). DOI: 10.1002/adma.201902302.
(34) Pan, M.-A.; Lau, T.-K.; Tang, Y.; Wu, Y.-C.; Liu, T.; Li, K.; Chen, M.-C.; Lu, X.; Ma, W.; Zhan, C. 16.7%-Efficiency Ternary Blended Organic Photovoltaic Cells with PCBM as the Acceptor Additive to Increase the Open-Circuit Voltage and Phase Purity. *J. Mater. Chem. A* **2019**, *7* (36), 20713–20722. DOI: 10.1039/C9TA06929A.
(35) Galli, D.; Gasparini, N.; Forster, M.; Eckert, A.; Widling, C.; Killian, M. S.; Avgeropoulos, A.; Gregoriou, V. G.; Scherf, U.; Chochos, C. L.; Brabec, C. J.; Ameri, T. Suppressing the Surface Recombination and Tuning the Open-Circuit Voltage of Polymer/Fullerene Solar Cells by Implementing an Aggregative Ternary Compound. *ACS Appl. Mater. Interfaces* **2018**, *10* (34), 28803–28811. DOI: 10.1021/acsami.8b09174.
(36) Koster, L. J. A.; Mihailetchi, V. D.; Ramaker, R.; Blom, P. W. M. Light Intensity Dependence of Open-Circuit Voltage of Polymer:Fullerene Solar Cells. *Appl. Phys. Lett.* **2005**, *86* (12), 123509. DOI: 10.1063/1.1889240.
(37) Cowan, S. R.; Roy, A.; Heeger, A. J. Recombination in Polymer-Fullerene Bulk Heterojunction Solar Cells. *Phys. Rev. B* **2010**, *82* (24), 433. DOI: 10.1103/PhysRevB.82.245207.
(38) Goris, L.; Poruba, A.; Purkrt, A.; Vandewal, K.; Swinnen, A.; Haeldermans, I.; Haenen, K.; Manca, J. V.; Vaněček, M. Optical Absorption by Defect States in Organic Solar Cells. *J. Non-Cryst. Solids* **2006**, *352* (9-20), 1656–1659. DOI: 10.1016/j.jnoncrysol.2005.09.053.
(39) Goris, L.; Poruba, A.; Hod'ákova, L.; Vaněček, M.; Haenen, K.; Nesládek, M.; Wagner, P.; Vanderzande, D.; Schepper, L. de; Manca, J. V. Observation of the Subgap Optical Absorption in Polymer-Fullerene Blend Solar Cells. *Appl. Phys. Lett.* **2006**, *88* (5), 52113. DOI: 10.1063/1.2171492.

(40) Zhang, M.; Guo, X.; Ma, W.; Ade, H.; Hou, J. A Large-Bandgap Conjugated Polymer for Versatile Photovoltaic Applications with High Performance. *Adv. Mater.* **2015**, *27* (31), 4655–4660. DOI: 10.1002/adma.201502110.
(41) Stamm, M. Polymer Surface and Interface Characterization Techniques. In *Polymer Surfaces and Interfaces*; Stamm, M., Ed.; Springer Berlin Heidelberg, 2008; pp 1–16. DOI: 10.1007/978-3-540-73865-7_1.
(42) Schaffer, C. J.; Schlipf, J.; Dwi Indari, E.; Su, B.; Bernstorff, S.; Müller-Buschbaum, P. Effect of Blend Composition and Additives on the Morphology of PCPDTBT:$PC_{71}BM$ Thin Films for Organic Photovoltaics. *ACS Appl. Mater. Interfaces* **2015**, *7* (38), 21347–21355. DOI: 10.1021/acsami.5b05939.
(43) Wienhold, K. S.; Körstgens, V.; Grott, S.; Jiang, X.; Schwartzkopf, M.; Roth, S. V.; Müller-Buschbaum, P. Effect of Solvent Additives on the Morphology and Device Performance of Printed Nonfullerene Acceptor Based Organic Solar Cells. *ACS Appl. Mater. Interfaces* **2019**, *11* (45), 42313–42321. DOI: 10.1021/acsami.9b16784.
(44) Wienhold, K. S.; Chen, W.; Yin, S.; Guo, R.; Schwartzkopf, M.; Roth, S. V.; Müller-Buschbaum, P. Following in Operando the Structure Evolution-Induced Degradation in Printed Organic Solar Cells with Nonfullerene Small Molecule Acceptor. *Sol. RRL* **2020**, *4* (9). DOI: 10.1002/solr.202000251.
(45) Doumon, N. Y.; Houard, F. V.; Dong, J.; Christodoulis, P.; Dryzhov, M. V.; Portale, G.; Koster, L. J. A. Improved Photostability in Ternary Blend Organic Solar Cells: the Role of [70]PCBM. *J. Mater. Chem. C* **2019**, *5*, 13176. DOI: 10.1039/C8TC06621C.
(46) Zhu, Y.; Gadisa, A.; Peng, Z.; Ghasemi, M.; Ye, L.; Xu, Z.; Zhao, S.; Ade, H. Rational Strategy to Stabilize an Unstable High-Efficiency Binary Nonfullerene Organic Solar Cells with a Third Component. *Adv. Energy Mater.* **2019**, *9* (20), 1900376. DOI: 10.1002/aenm.201900376.
(47) Tremolet de Villers, B. J.; O'Hara, K. A.; Ostrowski, D. P.; Biddle, P. H.; Shaheen, S. E.; Chabinyc, M. L.; Olson, D. C.; Kopidakis, N. Removal of Residual Diiodooctane Improves Photostability of High-Performance Organic Solar Cell Polymers. *Chem. Mater.* **2016**, *28* (3), 876–884. DOI: 10.1021/acs.chemmater.5b04346.
(48) Doumon, N. Y.; Wang, G.; Qiu, X.; Minnaard, A. J.; Chiechi, R. C.; Koster, L. J. A. 1,8-Diiodooctane Acts as a Photo-Acid in Organic Solar Cells. *Scientific reports* **2019**, *9* (1), 4350. DOI: 10.1038/s41598-019-40948-1. Published Online: Mar. 13, 2019.
(49) Classen, A.; Heumueller, T.; Wabra, I.; Gerner, J.; He, Y.; Einsiedler, L.; Li, N.; Matt, G. J.; Osvet, A.; Du, X.; Hirsch, A.; Brabec, C. J. Revealing Hidden UV Instabilities in Organic Solar Cells by Correlating Device and Material Stability. *Adv. Energy Mater.* **2019**, *9* (39), 1902124. DOI: 10.1002/aenm.201902124.
(50) Vandewal, K.; Benduhn, J.; Nikolis, V. C. How to Determine Optical Gaps and Voltage Losses in Organic Photovoltaic Materials. *Sustainable Energy Fuels* **2018**, *2* (3), 538–544. DOI: 10.1039/C7SE00601B.
(51) Xu, Z. C.; Zhang, H. S.; Li, Z.; Yang, X. S.; Zhang, G. Theoretical Study on Electronic Structures and Spectroscopic Properties of Indene-C60 Monoadduct (ICMA). *AMR* **2012**, *535-537*, 1287–1290. DOI: 10.4028/www.scientific.net/AMR.535-537.1287.
(52) Souheng Wu. Calculation of Interfacial Tension in Polymer Systems. *J. Polymer. Sci.* **1971** (34), 19–30. DOI: 10.1002/polc.5070340105.
(53) Xu, Z.; Chen, L.-M.; Yang, G.; Huang, C.-H.; Hou, J.; Wu, Y.; Li, G.; Hsu, C.-S.; Yang, Y. Vertical Phase Separation in Poly(3-hexylthiophene): Fullerene Derivative Blends and its Advantage for Inverted Structure Solar Cells. *Adv. Funct. Mater.* **2009**, *19* (8), 1227–1234. DOI: 10.1002/adfm.200801286.

(54) Venkatesan, S.; Ngo, E.; Khatiwada, D.; Zhang, C.; Qiao, Q. Enhanced Lifetime of Polymer Solar Cells by Surface Passivation of Metal Oxide Buffer Layers. *ACS Appl. Mater. Interfaces* **2015**, *7* (29), 16093–16100. DOI: 10.1021/acsami.5b04687.
(55) Buffet, A.; Rothkirch, A.; Döhrmann, R.; Körstgens, V.; Abul Kashem, M. M.; Perlich, J.; Herzog, G.; Schwartzkopf, M.; Gehrke, R.; Müller-Buschbaum, P.; Roth, S. V. P03, the Microfocus and Nanofocus X-Ray Scattering (MiNaXS) Beamline of the PETRA III Storage Ring: the Microfocus Endstation. *J. Synchrotron Radiat.* **2012**, *19*, 647–653. DOI: 10.1107/S0909049512016895.
(56) Jiang, Z. GIXSGUI : a MATLAB Toolbox for Grazing-Incidence X-Ray Scattering Data Visualization and Reduction, and Indexing of Buried Three-Dimensional Periodic Nanostructured Films. *J Appl Crystallogr* **2015**, *48* (3), 917–926. DOI: 10.1107/S1600576715004434.

For Tables of Content Only: